

Experimental Research in the Aspect of Determining the Mechanical and Strength Properties of the Composite Material Made of Carbon-Epoxy Composite

Patryk Różyło^{1*}, Wojciech Smagowski¹, Jakub Paśnik¹

¹ Faculty of Mechanical Engineering, Lublin University of Technology, ul. Nadbystrzycka 36, 20-618 Lublin, Poland

* Corresponding author's e-mail: p.rozylo@pollub.pl

ABSTRACT

The present paper, provides a study of conducting experimental investigations (based on the ISO standards), in the context of determining material properties (mechanical and strength parameters) in the case of thin-walled composite structures – made of carbon-epoxy composite. Tests were carried out on 5 different types of test specimens (in accordance with the standards), with a minimum of 9 specimens per each type of test. The tests provided high repeatability of results, and the large number of test specimens per each test made it possible to precisely average the test results in terms of determining the necessary material properties. The tests were carried out using a Zwick Z100 universal testing machine (UTM), under room temperature conditions, using two types of test heads that allow static experimental tests. The results presented in this paper constitute a prelude to research within the framework of the project from the National Science Centre (Poland) with the number 2021/41/B/ST8/00148. The paper presents the initial stage of the implementation of the aforementioned project – which was the determination of material parameters of the composite material from which the target thin-walled composite structures with closed sections were made. The purpose of this paper was mainly to present a methodology for the determination of material parameters describing a composite material (laminate), in order to allow subsequent implementation of the determined properties into numerical models.

Keywords: material properties, laminates, strength testing, thin-walled composite structures

INTRODUCTION

Composite materials represent a modern type of engineering materials, with major applications in the aerospace, construction or automotive industries. The aforementioned group of materials, especially in the context of thin-walled composite structures – such as laminates, is a current subject of engineering research [1–3]. Their use in various industries is primarily due to the fact that such materials are characterized by the fact that they are very strong while keeping their own weight low [4–5]. In addition, thin-walled composite structures, made of a composite material such as carbon-epoxy composite, demonstrate special behavior under axial compression [6–8].

In short, they undergo a loss of stability (buckling) [9–11]. The buckling phenomenon is based on the fact that there is a change in the form of deformation of the structure [12–14]. The present phenomenon represents a special type of phenomenon that many researchers are currently dealing with [15–17]. It is important, to conduct interdisciplinary as well as in-depth research, especially during behaviors directly leading to loss of stability [18–20]. The behavior of the structure after buckling remains a challenge for a wide range of researchers and requires careful interpretation [21–23]. The desirable behavior is the case where, in the framework of the post-buckling behavior of the structure, there is a situation where the increase in deflection of the structure is

accompanied by an increase in compressive load [24–26]. The aforementioned behavior occurs in most of the scientific research conducted [27–29]. Besides investigating the buckling phenomenon, it is also important to study the phenomena that occur after buckling – where the structure is exposed to damage [30–32]. Usually, the analysis of the behavior of the structure in the post-buckling state under further axial compression, leads to the observation of complex forms of structural damage [33–35]. Recently, researchers have been concerned with analyzing complex forms of damage – thoroughly analyzing the aspect of loss of load-carrying capacity of structures [35–37]. Depending on the demand, it is possible to design composite structures that demonstrate higher energy consumption, or higher stiffness – if only by changing the arrangement of the constituent layers of the composite material [25,31]. Consequently, it is important to correctly determine the material properties of composite structures that are ultimately subjected to the above-described tests.

Composite materials represent a special group of materials, characterized by outstanding strength properties. It is important to conduct research on composite materials such as fiber reinforced polymer composite, to which include: CFRP, GFRP and BFRP. Structures made of materials of this type are characterized primarily by such properties as: light weight, high strength, excellent mechanical/fatigue properties, corrosion resistance, etc. The above-mentioned issues, among others, were presented in the papers [38–40].

In the current work, the main focus was on presenting the methodology for the correct determination of the properties of the composite material, within the framework of specially prepared test specimens, enabling the determination of a number of material parameters of the composite material (carbon-epoxy composite) [41]. Determination of material parameters was based on tests conducted in accordance with the standards under consideration (in this regard) [42–44]. The above, made it possible to determine the material properties characterized by the final composite test specimens with closed sections – manufactured under the project No. 2021/41/B/ST8/00148 financed by the National Science Centre (Poland).

In this paper, only a number of material parameters were determined (based on specially prepared specimens for static testing to determine the properties of the composite material), which were characterized by thin-walled composite

structures manufactured mainly for load-carrying capacity tests, presented in the final part of the paper. The reliability and accuracy of the experimental results presented in the paper, is determined by the high level of repeatability of the test results between the conducted experimental tests. A minimum of 9 test specimens were used within each type of test trials – which positively influenced the determination of average values from the determined parameters (that constitute the basic properties of the composite material). Each test was conducted in accordance with guidelines derived from ISO standards, maintaining a high level of accuracy and repeatability of testing. The determined material data will be the basis for further research, primarily in the context of FEM simulations [45–48].

The novelty of the present research was primarily the presentation of a comprehensive description of the determination of the necessary properties of the composite material (laminate) based on the standards under consideration.

MATERIALS AND METHODS

The test specimens under study were specially prepared test samples manufactured in accordance with the appropriate ISO standards (static tensile [42], shear [43] and compressive [44]). The specimens were prepared in accordance with the guidelines presented in the standards, which precisely defined the geometrical parameters of each specimen depending on the type of strength test to which the specimen was to be subjected (In Figures 1a and 1b, the specimens were characterized by the dimensions (length × width × thickness): $250 \times 15 \pm 0.5 \times 1 \pm 0.2$ mm and $175 \times 25 \pm 0.5 \times 2 \pm 0.2$ mm. In Figure 2, the specimens were characterized by dimensions: $250 \times 25 \pm 0.5 \times 2 \pm 0.2$ mm. In Figures 3a and 3b, the specimens were characterized by dimensions: $140 \times 10 \pm 0.5 \times 2 \pm 0.2$ mm and $140 \times 25 \pm 0.5 \times 2 \pm 0.2$ mm). Consequently, a number of composite specimens were prepared, made of carbon-epoxy composite, which allowed further determination of material properties.

All composite specimens were fabricated using the autoclave technique (both the material test specimens presented in this paper and the target thin-walled composite structures with closed sections, shown in Fig. 10). All specimens were manufactured from unidirectional CYCOM 985–42%-HS-135–305 prepreg tape, where the

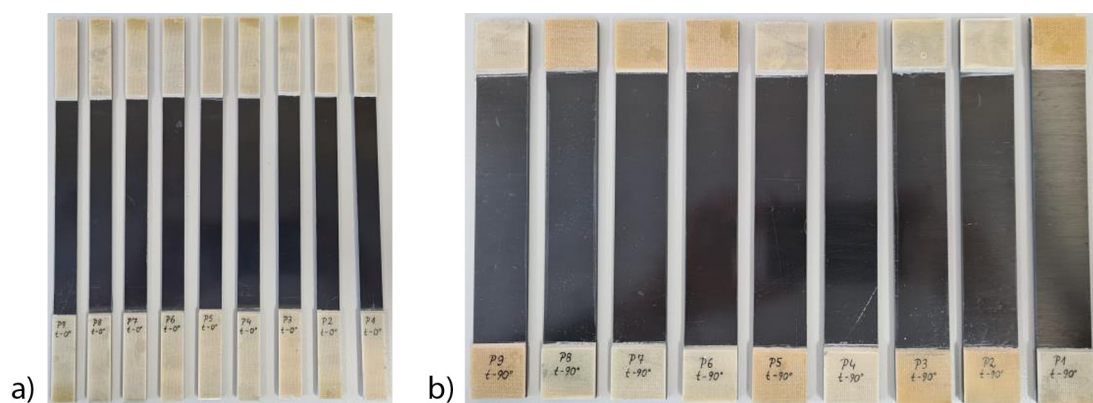


Figure 1. Specimens for determining material properties in static tensile testing: (a) first specimens type, (b) second specimens type

resin system constituted 42% of the material volume, while the high-strength fibers are characterized by a grammage of 135 g/m². The basic width of the prepreg tape was 305 mm. All specimens were cured in an autoclave at a temperature of 177 °C and an overpressure of 0.6 MPa.

The specimens prepared for the static tensile test, were produced in accordance with PN-EN ISO 527-5 (of 2010) [42] – the equivalent was ASTM D 3039. In addition, there were two different types of such specimens, due to the fact that the static tensile test involved both composite specimens, where the fibers were arranged along the tensile direction (P1÷P9 t-0°) and in the direction transverse to the tensile direction (P1÷P9 t-90°) – as shown in Figure 1. Another type of specimens were those intended for static

shear testing, and were made in accordance with PN-EN ISO 14129 (of 2000) [43] – the equivalent was ASTM D 3518. These specimens were mainly characterized by the fact that the fibers in the layers of the composite material were arranged in a direction of ±45° with respect to the tensile direction (P1÷P9 shr-45°) – these specimens are presented in Figure 2. The last type of specimens for determining the properties of the composite material were those intended for static compressive testing, which were produced in accordance with PN-EN ISO 14126 (of 2002) [44] – the equivalent was ASTM D 3410. These specimens, like the specimens for the static tensile test, occurred in two types – with the first type of specimens characterized by the composite material’s fibers being arranged along the compressive

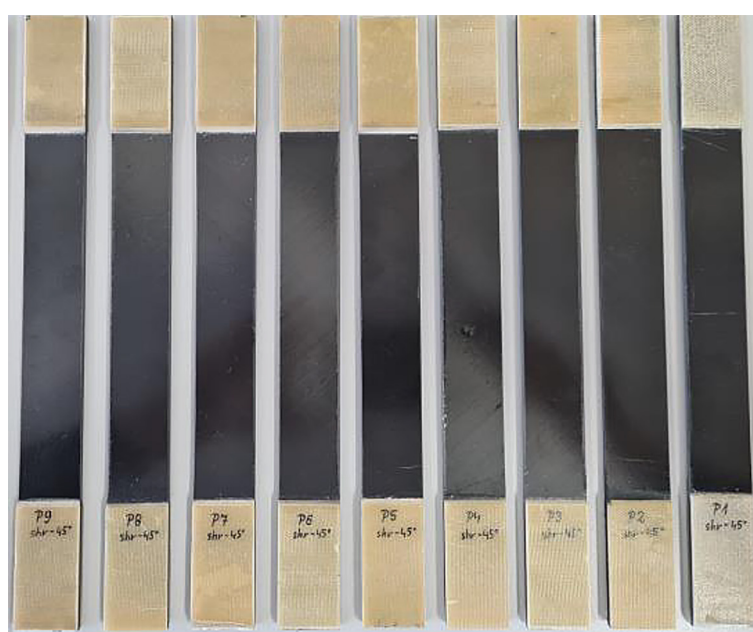


Figure 2. Specimens for determining material properties in static shear testing

direction (P1÷P10 c-0°), and the second case being specimens with fibers arranged transverse to the compressive direction (P1÷P9 c-90°) – as shown in Figure 3.

As shown in Figs. 1–3, a number of specimens were produced to determine the material properties of the composite material. For most types of static tests, a total of 9 test specimens each were produced (Figs. 1,2 and 3b), while for the static compressive test, where the specimens were characterized by the fact that the fibers were arranged along the compressive direction (Fig. 3a), there were 10 such specimens. The large number of prepared specimens made it possible to perform a number of tests in static compressive tests, which enabled the precise determination of a number of material parameters of the carbon-epoxy composite. During the process of determining the material properties of the carbon-epoxy composite, the necessary accessories were provided, enabling, among other things, the correct execution of experimental tests. The accessories included electro-resistance strain gauges (of TENMEX companies) and small laboratory equipment, enabling, in particular, the correct attachment of the electro-resistance strain gauges to the test specimens. Figure 4 shows the accessories for the test specimens.

After the test specimens were prepared for strength testing, all kinds of static tests were started to determine the properties of the composite material. Directly mounted strain gauges, according to the standards, allowed, among other things, further registration of deformations in the longitudinal and transverse directions – depending on the type of test specimens. All experimental tests, were carried out using a Zwick Z100 (Zwick Roell GmbH & Co. KG, Ulm, Germany) universal testing machine (at room temperature) – equipped with special grips that make it possible to carry out all types of tests to determine the properties of the composite material. The test stand was equipped with two types of special heads that made it possible to conduct both tests in the context of static tensile (2 mm/min) and compressive tests (1 mm/min). All tests were conducted under room temperature conditions. The test stand is shown in Figure 5.

In the first stage of the study, tests were carried out in order to determine properties such as Young’s Modulus in the fiber direction E_1 , Poisson’s ratio ν_{12} , tensile strength in the fiber direction F_{TU} (0°) and tensile failure force in the fiber direction (0°). For this purpose, a static tensile test was carried out for specially prepared test specimens in which the fibers were arranged according to the tensile direction (P1÷P9 t-0°) – Fig. 6a.

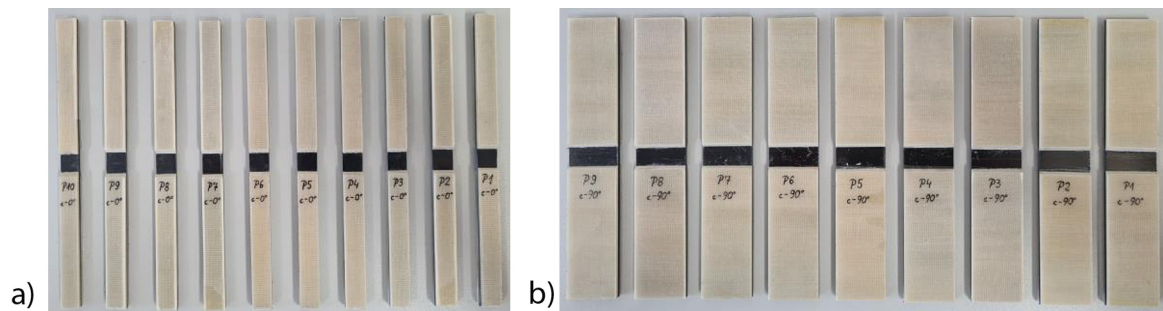


Figure 3. Specimens for determining material properties in static compressive testing: (a) first specimens type, (b) second specimens type

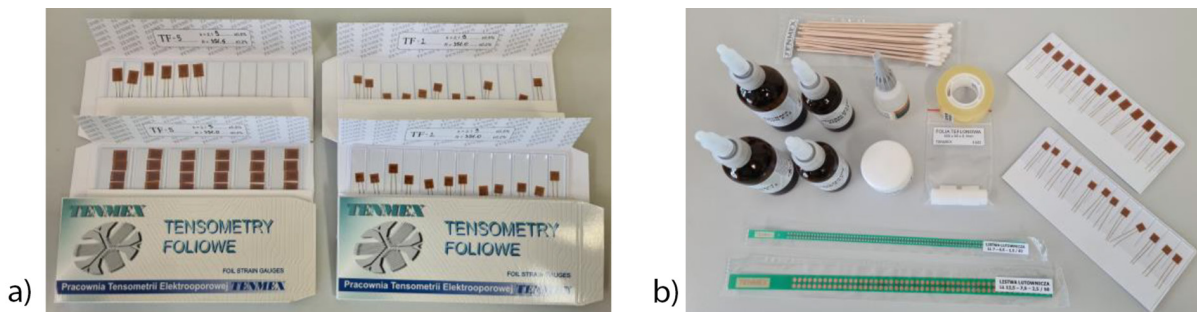


Figure 4. Necessary accessories for test specimens: (a) strain gauges, (b) other accessories

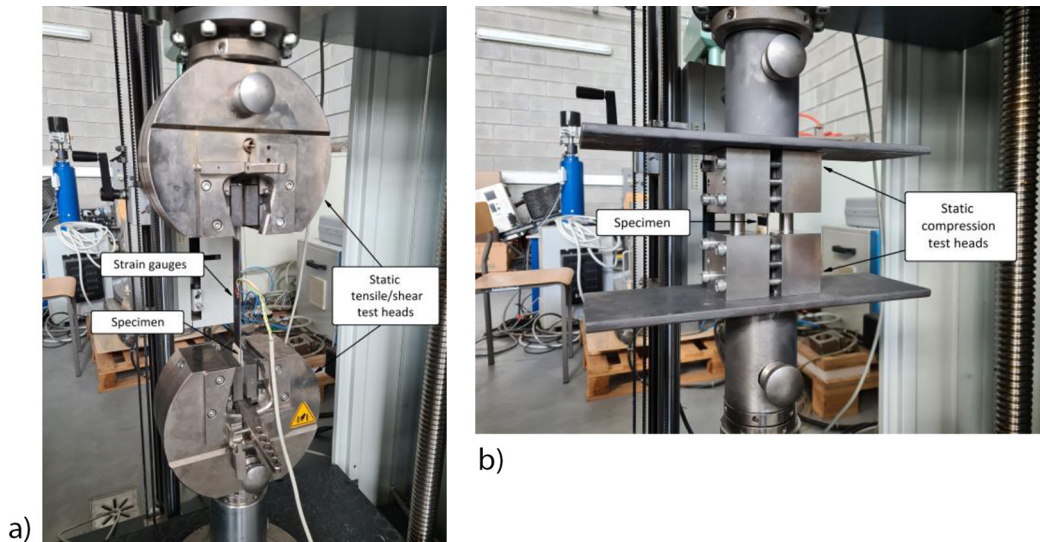


Figure 5. Test stand: (a) with heads for static tensile testing, (b) with heads for static compressive testing

Young’s modulus E_1 was determined in from the following relationship:

$$E_1 = \frac{\sigma'' - \sigma'}{\varepsilon_l'' - \varepsilon_l'} \quad (1)$$

where: σ' – stress measured at longitudinal strain $\varepsilon_l' = 0.05\%$,
 σ'' – stress measured at longitudinal strain $\varepsilon_l'' = 0.25\%$.

The stress was determined according to the following relation:

$$\sigma = \frac{P}{A} \quad (2)$$

where: P – load (P' and P'' respectively for $\varepsilon_l' = 0.05\%$ and $\varepsilon_l'' = 0.25\%$),
 A – initial cross-sectional area (measured for each material test specimen).

The (average value of) Poisson’s ratio ν_{12} , which is the ratio of transverse to longitudinal strain, was determined from the following relationship:

$$\nu_{12} = \frac{\varepsilon_t'''}{\varepsilon_l'''} = \frac{1}{2} \left(\frac{\varepsilon_t'}{\varepsilon_l'} + \frac{\varepsilon_t''}{\varepsilon_l''} \right) \quad (3)$$

where: ε_t''' – values of transverse strains (ε_t' and ε_t''), corresponding to longitudinal strains ε_l''' (ε_l' and ε_l'') – respectively for $\varepsilon_l' = 0.05\%$ and $\varepsilon_l'' = 0.25\%$.

Tensile strength in the fiber direction $F_{TU}(0^\circ)$, was estimated according to the following relationship:

$$F_{TU(0^\circ)} = \frac{P_{max}}{A} \quad (4)$$

where: P_{max} – tensile failure force in the fiber direction (0°).

The above-described relationships (Eqs. 1–4) made it possible to determine the described material parameters.

Then, it was dealt with to perform tests to determine Young’s Modulus in the transverse direction to the fibers E_2 (which was determined from Eq. 1 as in the case of E_1), tensile strength in the transverse direction to the fibers $F_{TU}(90^\circ)$ – which was determined analogously to the tensile strength in the fiber direction, as in Eq. 4, as well as tensile failure force in the transverse direction to the fibers (90°) – Fig. 6b. The tests made it possible to determine all the parameters mentioned, using the specimens where the fibers were arranged in the transverse direction to the tensile ($P1 \div P9$ t- 90°).

Young’s modulus E_2 was determined in from the following relationship:

$$E_2 = \frac{\sigma'' - \sigma'}{\varepsilon_l'' - \varepsilon_l'} \quad (5)$$

Tensile strength in the transverse direction to the fibers $F_{TU}(90^\circ)$, was estimated according to the following relationship:

$$F_{TU(90^\circ)} = \frac{P_{max}}{A} \quad (6)$$

where: P_{max} – tensile failure force in the transverse direction to the fiber (90°).

Both above-mentioned types of tests (tests determining tensile strength) were conducted based on the guidelines and procedure outlined in the PN-EN ISO 527–5 (of 2010) standard.

In the next step, a static strength test was conducted to determine material properties such as Kirchhoff coefficient G_{12} , shear strength F_{SU} ($\pm 45^\circ$) and shear failure force. The Kirchhoff coefficient was determined according to the following relationship:

$$G_{12} = \frac{\tau''_{12} - \tau'_{12}}{\gamma''_{12} - \gamma'_{12}} \quad (7)$$

where: τ'_{12} – is the shear stress at the shear strain $\gamma'_{12} = 0.1\%$,
 τ''_{12} – is the shear stress at the shear strain $\gamma''_{12} = 0.5\%$.

The shear stress τ_{12} presented in Eq. (7) was determined using equation:

$$\tau_{12} = \frac{P}{2 \cdot A} \quad (8)$$

where: P – load (P' and P'' respectively for $\gamma'_{12} = 0.1\%$ and $\gamma''_{12} = 0.5\%$),
 A – initial cross-sectional area (measured for each material test specimen).

The shear strain follows the relationship:

$$\gamma_{12} = \varepsilon_l - \varepsilon_t \quad (9)$$

where: ε_l – strain in the parallel (longitudinal) direction to the axis of the specimen,
 ε_t – strain in the perpendicular (transverse) direction to the axis of the specimen.

Furthermore, the shear ultimate strength was determined from the following equation:

$$F_{SU(\pm 45^\circ)} = \frac{P_{max}}{2 \cdot A} \quad (10)$$

where: P_{max} – shear failure force.

The above parameters were determined using the example of specimens (P1÷P9 shr-45°) in which the fibers were arranged at an angle $\pm 45^\circ$ – and the test specimens were carried out based on a PN-EN ISO 14129 (of 2000) standard, that allows the determination of parameters related to the shear of the composite – Fig. 6c.

Moreover, experimental tests were carried out to determine compressive-related properties of the composite: compressive strength in the fiber direction F_{CU} (0°) and compressive failure force. Tests were conducted on specially prepared test specimens (P1÷P10 c-0°) – Fig. 6d. A similar procedure was used to determine compressive parameters for specimens in which the fibers were arranged transversely to the direction of compressive (P1÷P9 c-90°) – where the compressive strength in the transverse direction to the fibers F_{CU} (90°) and the failure force (in the same direction) were determined – Fig. 6e.

Compressive strength in the fiber direction F_{CU} (0°), was estimated according to the following relationship:

$$F_{CU(0^\circ)} = \frac{P_{max}}{A} \quad (11)$$

where: P_{max} – compressive failure force in the fiber direction (0°).

Compressive strength in the transverse direction to the fibers F_{CU} (90°), was estimated according to the following relationship:

$$F_{CU(90^\circ)} = \frac{P_{max}}{A} \quad (12)$$

where: P_{max} – compressive failure force in the transverse direction to the fibers (90°).

Both types of tests (tests determining compressive strength) were conducted based on the guidelines and procedure outlined in the PN-EN ISO 14126 (of 2002) standard.

All guidelines and the method of determining the material properties are presented in the aforementioned standards – tests were conducted in accordance with the guidelines.

After the completed experimental tests, carried out until the failure of the test specimens for material testing, the determination of material properties was addressed – which was performed according to the guidelines contained in the standards.

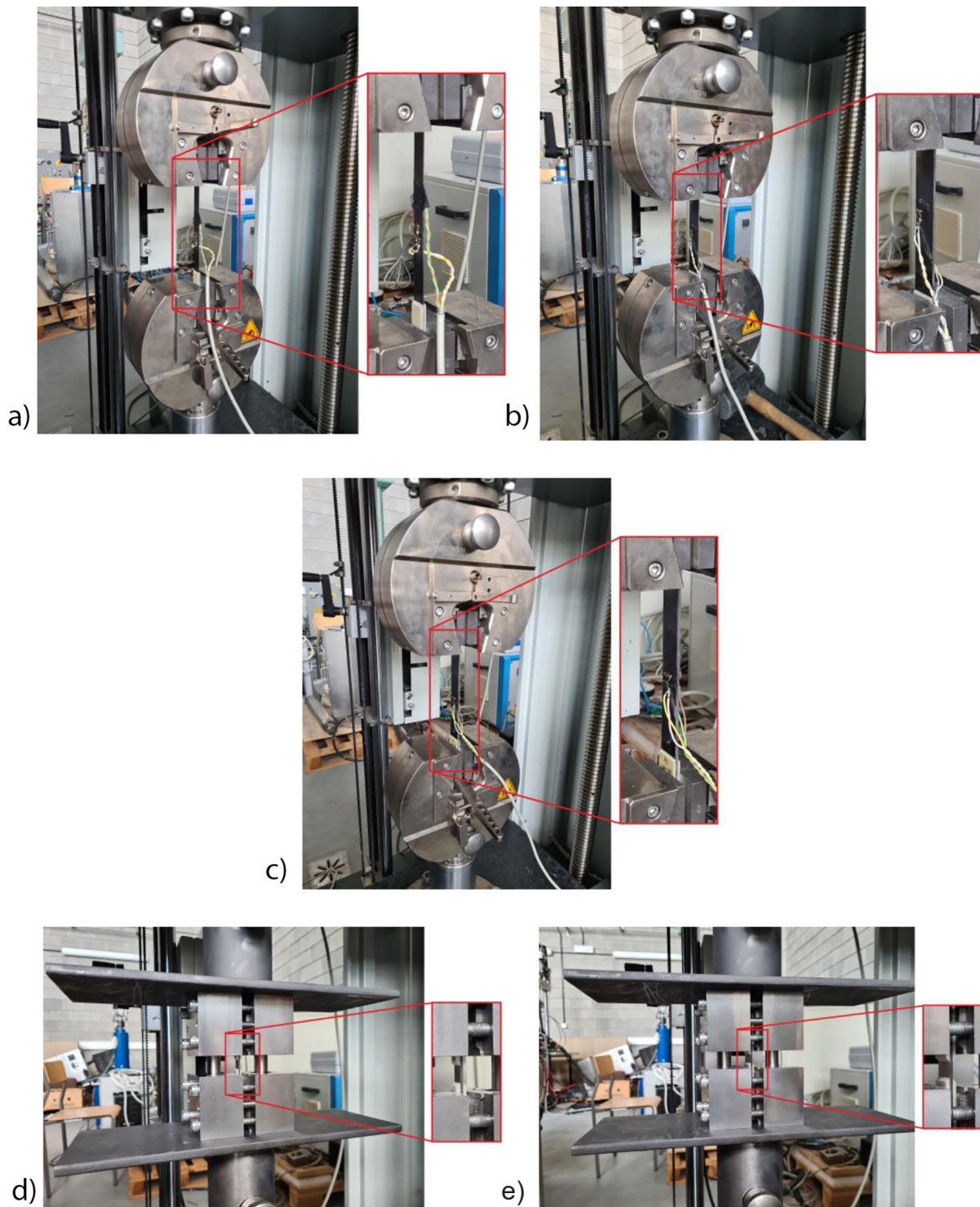


Figure 6. Static strength tests: (a) specimens (P1÷P9 t-0°), (b) specimens (P1÷P9 t-90°), (c) specimens (P1÷P9 shr-45°), (d) specimens (P1÷P10 c-0°), (e) specimens (P1÷P9 c-90°)

RESULTS AND DISCUSSION

On the basis of the tests carried out, both experimental characteristics, such as force-time, obtained directly from the testing machine, as well as characteristics that depend on load on strain (based on strain gauges mounted on the

specimens) were obtained – thus determining the desired material parameters.

Based on the characteristics, presented in Figure 7, it was possible to directly assess the limit loads (P_{max} – maximum loads for each specimen type) – at which the failure of each specimen occurred. The above, made it possible to determine

the material parameters of the composite material, related to tensile (for specimens P1÷P9 t-0° and P1÷P9 t-90°), shear (for specimens P1÷P9 shr-45°) and compressive (for specimens P1÷P10 c-0° and P1÷P9 c-90°) strength. The strength parameters based on the Eqs. (4,6,10–12), were estimated for all specimens identically, which was the ratio of the maximum registered load to the initial cross-sectional area of the specimen.

Figure 8 presents the load-strain characteristics, taking selected test specimens as an example. Based on the example specimens (Figure 8), the approximate values of the mechanical parameters of the composite material were estimated. For this purpose, to determine the Young's Modulus E_1 from the characteristics shown in Figure 8a,

the load values P (P' and P'') were read for both values of longitudinal strains ($\epsilon'_t = 0.05\%$ and $\epsilon''_t = 0.25\%$). Then, the stresses values σ (σ' and σ'') were determined as a ratio of the read load values P (P' and P''), relative to the initial cross-sectional area value A of specimen – according to Eq. (1). Thus, it was possible to further determine the parameter $E_1 = 104,232.93$ MPa – for specimen P1 t-0°. In order to determine the Poisson's ratio, it was necessary to read the values of transverse strains (ϵ'_t and ϵ''_t), corresponding to both values of longitudinal strains ($\epsilon'_t = 0.05\%$ and $\epsilon''_t = 0.25\%$) – according to Eq. (3). After dividing the corresponding strains with respect to each other, it is necessary to determine the average value from the sum of these expressions – through

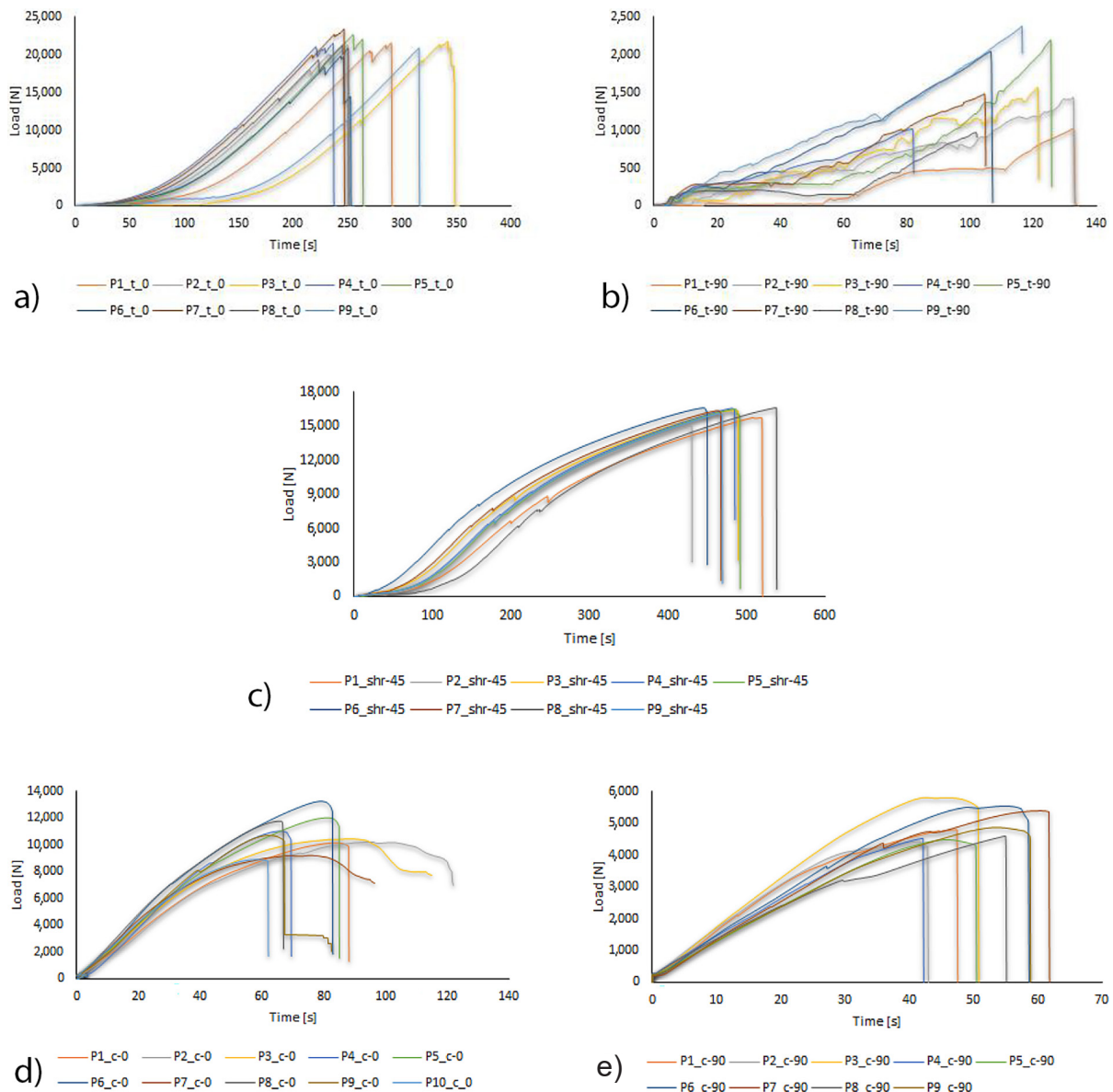


Figure 7. Failure characteristics: (a) specimens (P1÷P9 t-0°), (b) specimens (P1÷P9 t-90°), (c) specimens (P1÷P9 shr-45°), (d) specimens (P1÷P10 c-0°), (e) specimens (P1÷P9 c-90°)

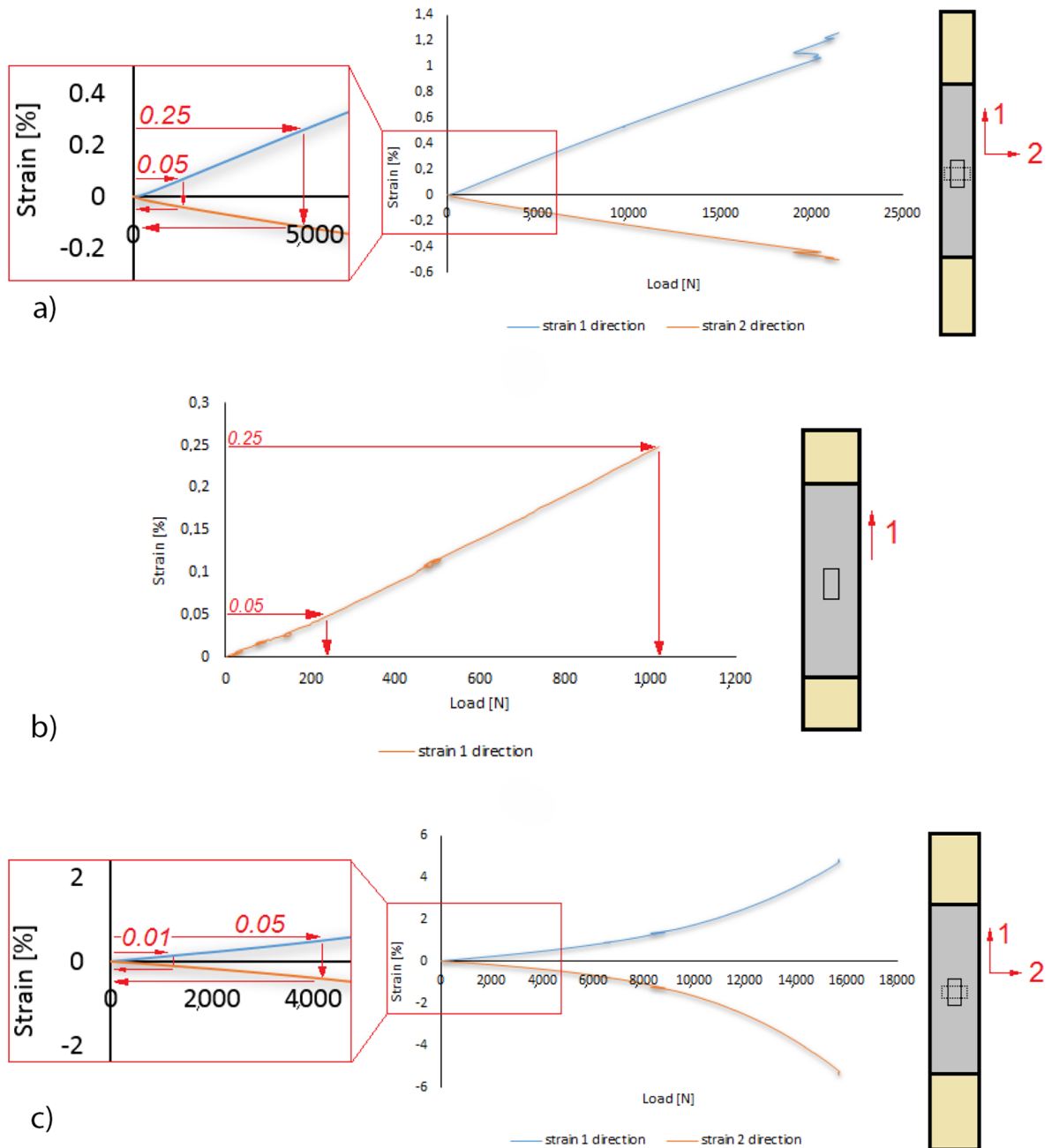


Figure 8. Load-strain characteristics: (a) for specimen P1 $t-0^\circ$ where the fibers are arranged along the tensile direction, (b) for specimen P1 $t-90^\circ$ where the fibers are arranged transversely to the tensile direction, (c) for specimen P1 shr- 45° where fibers were arranged at an angle $\pm 45^\circ$ to the tensile direction

which the desired parameter will be determined. This made it possible to determine the parameter $\nu_{12} = 0.58$ – for specimen P1 $t-0^\circ$. Young’s Modulus in the transverse direction to the fibers E_2 was determined according to the example characteristics presented in Figure 8b. This parameter was determined identically to Young’s Modulus E_1 – according to Eq. (5). The value of the determined Young’s Modulus for specimen P1 $t-90^\circ$ was equal $E_2 = 7751.28$ MPa. The last of the important mechanical parameters was the Kirchhoff Modulus

G_{12} . This parameter was determined in a similar manner to the previously described Young’s modulus. This parameter constituted the ratio of the difference in shear stresses ($\tau''_{12} - \tau'_{12}$), relative to the difference in shear strains ($\gamma''_{12} - \gamma'_{12}$) – according to equation (7). The shear strains are respectively: $\gamma'_{12} = 0.1\%$ and $\gamma''_{12} = 0.5\%$. The method of determining shear stresses is according to Eq. (8). The above approach, made it possible to determine the Kirchhoff Modulus $G_{12} = 4194.04$ MPa – for specimen P1 shr- 45° .

The above-described method of determining basic mechanical properties, made it possible to determine the mentioned properties for all test specimens in the same manner. All experimental tests were conducted over the full load range until the specimens were fully damaged – as shown in the example test results presented in Figure 9.

All of the above presented test results and the methodology for conducting these tests, contributed to the determination of all material parameters of the carbon-epoxy composite, both in terms of mechanical and strength properties. The material properties determined for all specimens for material testing are shown in Tab. 1.

The averaged values of strength and mechanical properties of the composite material (CYCOM 985-42%-HS-135-305 TENAX HTA) are presented in Table 2 as average values, and the standard deviation shown in brackets. Standard deviation provides a measure of how widely values are dispersed from the average (mean) value.

The determined mechanical properties made it possible to obtain information in terms of material parameters, within the framework of the

actual test specimens – which were thin-walled composite columns with closed sections, made as part of research conducted under the project No. 2021/41/B/ST8/00148 financed by the National Science Centre (Poland). In the case of implementation of target tests on composite structures with closed sections as well as within the framework of FEM simulations, besides the results obtained from the average values, the standard deviation that was obtained will be also considered. Implementation of test results in future numerical models, will take into consideration not only the obtained average values, but also the standard deviation, which is very significant. The above will make it possible to ensure the correctness of the FEM simulation results obtained in the future, both in quantitative and qualitative aspects. Figure 10 presents only sample test profiles for which a methodology for determining material properties has been presented.

The obtained material parameters (both mechanical and strength), which are summarized in Table 1, provide the basis for further research – on target thin-walled composite



Figure 9. Damaged specimens for material testing: (a) specimens P1÷P9 t-0°, (b) specimens P1÷P9 shr-45°, (c) specimens P1÷P9 c-90°

Table 1. Properties of the composite material.

Specimen	E_1	E_2	G_{12}	ν_{12}	P_{max}	$F_{TU}(0^\circ)$	$F_{SU}(45^\circ)$	$F_{TU}(90^\circ)$	$F_{CU}(0^\circ)$	$F_{CU}(90^\circ)$
	MPa	MPa	MPa	-	N	MPa	MPa	MPa	MPa	MPa
P1_t-0°	104,232.93			0.58	21,541.77	1,295.96				
P2_t-0°	103,360.62			0.22	21,284.17	1,294.53				
P3_t-0°	107,602.69			0.33	21,758.10	1,299.25				
P4_t-0°	100,129.22			0.20	21,499.04	1,259.08				
P5_t-0°	101,535.27			0.61	22,635.34	1,337.15				
P6_t-0°	103,437.31			0.47	19,807.16	1,179.55				
P7_t-0°	101,692.76			0.16	23,378.80	1,372.90				
P8_t-0°	100,844.06			0.22	21,220.94	1,235.53				
P9_t-0°	104,292.10			0.51	20,892.50	1,222.73				
Average value	103,014.11			0.37	21,557.53	1,277.41				
Standard deviation	2,145.73			0.17	955.49	56.23				
P1_shr-45°			4,194.04		15,744.48		135.58			
P2_shr-45°			4,404.15		15,022.68		129.39			
P3_shr-45°			3,939.33		16,353.93		136.76			
P4_shr-45°			3,859.24		16,552.89		135.55			
P5_shr-45°			4,103.01		16,485.60		135.06			
P6_shr-45°			4,036.57		16,582.55		137.42			
P7_shr-45°			3,949.94		16,348.02		132.48			
P8_shr-45°			3,837.99		16,605.18		137.15			
P9_shr-45°			4,040.47		16,133.39		130.95			
Average value			4,040.53		16,203.19		134.48			
Standard deviation			167.35		489.91		2.71			
P1_t-90°		7,751.28			1,020.05			20.35		
P2_t-90°		7,244.27			1,436.25			28.18		
P3_t-90°		7,200.66			1,566.64			31.23		
P4_t-90°		7,655.20			1,017.19			20.48		
P5_t-90°		6,746.87			2,193.23			43.17		
P6_t-90°		7,222.67			2,041.09			41.36		
P7_t-90°		7,755.23			1,481.90			30.34		
P8_t-90°		7,444.98			969.90			21.12		
P9_t-90°		7,231.91			2,375.47			46.88		
Average value		7,361.45			1,566.86			31.46		
Standard deviation		307.97			500.32			9.64		
P1_c-0°					10,142.22				562.51	
P2_c-0°					10,212.20				521.50	
P3_c-0°					10,441.75				598.48	
P4_c-0°					11,015.71				569.45	
P5_c-0°					12,008.66				609.11	
P6_c-0°					13,236.98				665.95	
P7_c-0°					9,204.59				496.69	
P8_c-0°					1,1752.95				599.59	
P9_c-0°					1,0706.29				565.52	
P10_c-0°					8,900.29				535.63	
Average value					10,762.16				572.44	

Table 1. Cont.

Specimen	E_1	E_2	G_{12}	ν_{12}	P_{max}	$F_{TU}(0^\circ)$	$F_{SU}(45^\circ)$	$F_{TU}(90^\circ)$	$F_{CU}(0^\circ)$	$F_{CU}(90^\circ)$
	MPa	MPa	MPa	-	N	MPa	MPa	MPa	MPa	MPa
Standard deviation					1,241.36				46.20	
P1_c-90°					4,795.56					106.49
P2_c-90°					4,420.60					93.21
P3_c-90°					5,802.14					117.86
P4_c-90°					4,522.92					96.67
P5_c-90°					4,484.22					101.62
P6_c-90°					5,540.99					110.45
P7_c-90°					5,387.96					109.71
P8_c-90°					4,593.10					98.24
P9_c-90°					4,865.42					102.10
Average value					4,934.77					104.04
Standard deviation					483.40					7.34

Table 2. Material properties of the carbon-epoxy composite (average values with standard deviation).

Mechanical parameters		Strength parameters	
Young's modulus E_1 [MPa]	103,014.11 (2,145.73)	Tensile strength $F_{TU}(0^\circ)$ [MPa]	1,277.41 (56.23)
Young's modulus E_2 [MPa]	7,361.45 (307.97)	Compressive strength $F_{CU}(0^\circ)$ [MPa]	572.44 (46.20)
Poisson's ratio ν_{12} [-]	0.37 (0.17)	Tensile strength $F_{TU}(90^\circ)$ [MPa]	31.46 (9.64)
Kirchhoff modulus G_{12} [MPa]	4,040.53 (167.35)	Compressive strength $F_{CU}(90^\circ)$ [MPa]	104.04 (7.34)
-	-	Shear strength $F_{SU}(45^\circ)$ [MPa]	134.48 (2.71)



Figure 10. Target test specimens for which material properties were determined

structures with closed sections. The aim of the present study, was primarily to determine the material parameters within the composite material from which the target thin-walled composite structures for stability and load-carrying tests were manufactured, with further in-depth

assessment of the failure phenomenon. The material properties determined by static experimental tests, will be implemented into numerical models (FEM). This will allow a faithful representation of the behavior of thin-walled structures modeled numerically – which will

enable further comparison of the results of stability and load-carrying capacity tests of structures with closed sections for both experimental and FEM tests.

CONCLUSIONS

Based on the research conducted in this paper, it was possible to determine the desired properties of the composite material – a carbon-epoxy composite (laminate). The research presented in this paper made it possible to present an approximate research methodology, allowing to determine approximate values of the composite material (average values with standard deviation), both for mechanical (elastic) and strength properties.

Based on the study and referring to average values, it was estimated that Young's modulus E_1 is approximately 14 times higher than Young's modulus E_2 – this indicates a significant discrepancy in the case of material stiffness depending on the direction of loading. Moreover, it can be observed, among other things, that the tensile strength in the fiber direction F_{TU} (0°) is 2.23 times higher than the compressive strength in the fiber direction F_{CU} (0°). In addition, the tensile strength in the direction transverse to the fibers F_{TU} (90°) relative to the compressive strength in the direction transverse to the fibers F_{CU} (90°) differs about 3.31 times. The above, confirms that composite materials are a special group of materials with significant differences in stiffness and strength depending on the direction of loading.

The determined material properties in the context of average values and standard deviations should be subjected to additional statistical processing or based on information presented in standards such as EN 1990. All future research and the final implementation of the determined approximate material properties into numerical models, will be further verified by the convergence of experimental results and FEM models. More detailed information on how to determine material parameters is presented in the work [41] – as mentioned in the introduction. In the literature, there is not enough papers on how to determine the properties of composite materials, since all the methodology is contained in standards. The current paper deals with the determination of a number of material parameters based on ISO standards [42–44].

Acknowledgments

The research presented in the paper, provides the basis for the research conducted under the project No. 2021/41/B/ST8/00148, financed by the National Science Centre (Poland) – on load-carrying capacity of composite profiles with closed sections, using interdisciplinary research techniques.

REFERENCES

- Berardi, V.P.; Perrella, M.; Feo, L.; Cricri, G. Creep behavior of GFRP laminates and their phases: Experimental investigation and analytical modeling. *Compos. Part B Eng.* 2017; 122: 136–144. <https://doi.org/10.1016/j.compositesb.2017.04.015>
- Fascetti, A.; Feo, L.; Nistic, N.; Penna, R. Web-flange behavior of pultruded GFRP I beams: A lattice model for the interpretation of experimental results. *Compos. B Eng.* 2016; 100: 257–269.
- Falkowicz, K.; Debski, H. Stability analysis of thin-walled composite plate in unsymmetrical configuration subjected to axial load. *Thin-Walled Structures*, 2021, 158, 107203.
- Rozylo, P.; Wysmulski, P. Failure analysis of thin-walled composite profiles subjected to axial compression using progressive failure analysis (PFA) and cohesive zone model (CZM). *Compos. Struct.* 2021; 262: 113597. <https://doi.org/10.1016/j.compstruct.2021.113597>
- Rozylo, P.; Debski, H. Effect of eccentric loading on the stability and load-carrying capacity of thin walled composite profiles with top-hat section. *Compos. Struct.* 2020; 245: 112388.
- Banat, D.; Mania, R. Failure assessment of thin-walled FML profiles during buckling and post-buckling response. *Compos. Part B: Eng.* 2017; 112: 278–289. <https://doi.org/10.1016/j.compositesb.2017.01.001>
- Madukauwa-David, I.D.; Drissi-Habti, M. Numerical simulation of the mechanical behavior of a large smart composite platform under static loads. *Compos. Part B Eng.* 2016; 88: 19–25. <https://doi.org/10.1016/j.compositesb.2015.10.041>
- Feo, L.; Latour, M.; Penna, R.; Rizzano, G. Pilot study on the experimental behavior of GFRP-steel slip-critical connections. *Compos. Part B Eng.* 2017; 115: 209–222. <https://doi.org/10.1016/j.compositesb.2016.10.007>
- Debski, H.; Rozylo, P.; Wysmulski, P.; Falkowicz, K.; Ferdynus, M. Experimental study on the effect of eccentric compressive load on the stability and load-carrying capacity of thin-walled composite profiles. *Compos. B Eng* 2021; 226: 109346.

10. Rozylo, P. Failure analysis of thin-walled composite structures using independent advanced damage models. *Compos. Struct.* 2021; 262: 113598. <https://doi.org/10.1016/j.compstruct.2021.113598>
11. Czechowski, L.; Kolakowski, Z. The study of buckling and post-buckling of a step-variable FGM box. *Materials* 2019; 12(6): 918.
12. Teter A. and Kolakowski Z.: Interactive buckling of wide plates made of Functionally Graded Materials with rectangular stiffeners. *Thin-Walled Struct.* 2022; 171: 108750.
13. Liu, J.; He, B.; Ye, W.; Yang, F. High performance model for buckling of functionally graded sandwich beams using a new semi-analytical method. *Compos. Struct.* 2021; 262: 113614.
14. Rozylo, P.; Lukasik, D. Numerical analysis of the critical state of thin-walled structure with z-profile cross section. *Adv. Sci. Technol. Res. J.* 2017; 11(1): 194–200.
15. Rozylo, P.; Falkowicz, K.; Wymulski, P.; Debski, H.; Pasnik, J.; Kral, J. Experimental-Numerical Failure Analysis of Thin-Walled Composite Columns Using Advanced Damage Models. *Materials* 2021; 14: 1506. <https://doi.org/10.3390/ma14061506>
16. Aveiga, D.; Ribeiro, M.L. A Delamination Propagation Model for Fiber Reinforced Laminated Composite Materials. *Math. Probl. Eng.* 2018; 2018: 1–9. <https://doi.org/10.1155/2018/1861268>
17. Gliszczynski, A.; Kubiak, T. Progressive failure analysis of thin-walled composite columns subjected to uniaxial compression. *Compos. Struct.* 2017; 169: 52–61.
18. Wymulski, P.; Debski, H. Post-Buckling and Limit States of Composite Channel-Section Profiles under Eccentric Compression. *Compos. Struct.* 2020; 245: 112356. <https://doi.org/10.1016/j.compstruct.2020.112356>
19. Rozylo, P. Experimental-numerical test of open section composite columns stability subjected to axial compression. *Arch. Mater. Sci. Eng.* 2017; 84(2): 58–64.
20. Rozylo, P.; Wrzesinska, K. Numerical analysis of the behavior of compressed thin-walled elements with holes. *Adv. Sci. Technol. Res. J.* 2016; 10(31): 199–206.
21. Falkowicz, K.; Debski, H. The work of a compressed, composite plate in asymmetrical arrangement of layers. *AIP Conf. Proc* 2019, 2078, 020005.
22. Falkowicz, K.; Debski, H.; Teter, A. Design solutions for improving the lowest buckling loads of a thin laminate plate with notch. *AIP Conf. Proc* 2018; 1922: 080004.
23. Wymulski, P.; Debski, H.; Falkowicz, K.; Rozylo, P. The influence of load eccentricity on the behavior of thin-walled compressed composite structures. *Compos. Struct.* 2019; 213: 98–107.
24. Falkowicz, K.; Debski, H. Stability analysis of thin-walled composite plate in unsymmetrical configuration subjected to axial load. *Thin-Walled Struct.* 2021; 158: 107203.
25. Rozylo, P. Stability and failure of compressed thin-walled composite columns using experimental tests and advanced numerical damage models. *Int J Numer Methods Eng.* 2021; 122: 5076–5099.
26. Kolanu, N.R.; Raju, G.; Ramji, M. A unified numerical approach for the simulation of intra and inter laminar damage evolution in stiffened CFRP panels under compression. *Compos. Part B Eng.* 2020; 190: 107931. <https://doi.org/10.1016/j.compositesb.2020.107931>
27. Li, W.; Cai, H.; Li, C.; Wang, K.; Fang, L. Progressive failure of laminated composites with a hole under compressive loading based on micro-mechanics. *Adv. Compos. Mater.* 2014; 23: 477–490. <https://doi.org/10.1080/09243046.2014.915105>
28. Rozylo, P. Comparison of Failure for Thin-Walled Composite Columns. *Materials* 2022, 15, 167.
29. Rozylo, P.; Wymulski, P.; Falkowicz, K. Fem and experimental analysis of thin-walled composite elements under compression. *Int. J. Appl. Mech. Eng.* 2017; 22(2): 393–402.
30. Duarte, A.P.C.; Díaz Sáez, A.; Silvestre, N. Comparative study between XFEM and Hashin damage criterion applied to failure of composites. *Thin Walled Struct.* 2017; 115: 277–288.
31. Rozylo, P. Experimental-numerical study into the stability and failure of compressed thin-walled composite profiles using progressive failure analysis and cohesive zone model. *Compos. Struct.* 2020; 257: 113303. <https://doi.org/10.1016/j.compstruct.2020.113303>
32. Rozylo, P.; Falkowicz, K. Stability and failure analysis of compressed thin-walled composite structures with central cut-out, using three advanced independent damage models. *Compos. Struct.* 2021; 273: 114298. <https://doi.org/10.1016/j.compstruct.2021.114298>
33. Ribeiro, M.L.; Vandepitte, D.; Tita, V. Damage Model and Progressive Failure Analyses for Filament Wound Composite Laminates. *Appl. Compos. Mater.* 2013; 20: 975–992. <https://doi.org/10.1007/s10443-013-9315-x>
34. Sohn, M.S.; Hu, X.Z.; Kim, J.K.; Walker, L. Impact damage characterisation of carbon fibre/epoxy composites with multilayer reinforcement. *Compos. B. Eng.* 2000; 31: 681–691.
35. Zhao, L.; Gong, Y.; Zhang, J.; Chen, Y.; Fei, B. Simulation of delamination growth in multidirectional laminates under mode I and mixed mode I/II

- loadings using cohesive elements. *Compos. Struct.* 2014; 116: 509–522. <https://doi.org/10.1016/j.compstruct.2014.05.042>.
36. Rzeczkowski, J.; Pasnik, J.; Samborski, S. Mode III numerical analysis of composite laminates with elastic couplings in split cantilever beam configuration. *Compos. Struct.* 2021; 265: 113751.
37. Tan, W.; Falzon, B.G.; Chiu, L.N.; Price, M. Predicting low velocity impact damage and Compression-After-Impact (CAI) behaviour of composite laminates. *Compos. Part A: Appl. Sci. Manuf.* 2015; 71: 212–226. <https://doi.org/10.1016/j.compositesa.2015.01.025>
38. Xian G., Guo R., Li C., Wang Y. Mechanical performance evolution and life prediction of prestressed CFRP plate exposed to hygrothermal and freeze-thaw environments. *Compos. Struct.* 2022; 293: 115719.
39. Subramanian N., Solaiyan E., Sendrayaperumal A., Lakshmaiya N. Flexural behaviour of geopolymer concrete beams reinforced with BFRP and GFRP polymer composites. *Advances in Structural Engineering* 2022; 25(5): 954–965.
40. Li C., Guo R., Xian G., Li H. Effects of elevated temperature, hydraulic pressure and fatigue loading on the property evolution of a carbon/glass fiber hybrid rod. *Polymer Testing* 2020; 90: 106761.
41. Ramkumar, R.; Rajaram, K.; Saravanan, P.; Venkatesh, R.; Saranya, K.; Jenaris, D.S. Determination of mechanical properties of CFRP composite reinforced with Abaca and Kenaf fibres. *Mater. Today: Proc.* 2022; 62: 5311–5316.
42. PN-EN ISO 527–5:2010.
43. PN-EN ISO 14129:2000.
44. PN-EN ISO 14126:2002.
45. Jonak, J.; Karpinski, R.; Wojcik, A.; Siegmund, M. The Influence of the Physical-Mechanical Parameters of Rock on the Extent of the Initial Failure Zone under the Action of an Undercut Anchor. *Materials* 2021; 14: 1841.
46. Jonak, J.; Siegmund, M.; Karpinski, R.; Wojcik, A. Three-Dimensional Finite Element Analysis of the Undercut Anchor Group Effect in Rock Cone Failure. *Materials* 2020; 13(6): 1332.
47. Jonak, J.; Karpinski, R.; Wojcik, A. Numerical Analysis of Undercut Anchor Effect on Rock. *J. Phys.: Conf. Ser.* 2021; 2130: 012011. <https://doi.org/10.1088/1742-6596/2130/1/012011>
48. Jonak, J.; Karpinski, R.; Wojcik, A. Numerical Analysis of the Effect of Embedment Depth on the Geometry of the Cone Failure. *J. Phys. Conf. Ser.* 2021; 2130: 012012. <https://doi.org/10.1088/1742-6596/2130/1/012012>